
AIRCRAFT FLIGHT SIMULATION

Ardrit Ramadani

DECEMBER 8, 2023

Abstract

This report carries out the simulation of an IMU utilizing the MatLab/SIMULINK block diagram package simulating the steady level flight between London and Amsterdam and London and Glasgow at 10km altitude over a time of flight of 1hr. The error prediction dynamics are factored to compare the measured data to the theoretically expected flight path. The measurements are found to have random noise errors as well as bias drift errors. A simulator exercise is also carried out in the CueSim Explorer RD F-16 simulator mounted on a Stewart platform to observe the Vestibulo-ocular effects and flight dynamics experienced by a pilot during flight. Where PIO and Type 1 spatial disorientation or observed to occur.

Contents

1. Introduction	2
2. Background.....	2
3. Block diagrams and subsystems	8
NED to navigation frame transformation subsystem.....	8
Angular velocity of the NED frame.....	8
NEV velocity from accelerations.....	9
Velocity to position calculations.....	9
Radius component calculations, R_E and R_N	10
Measured simulation block.....	10
Simulation of measured accelerations	11
4. Testing	12
5. Results	13
6. Discussion.....	15
7. Limitations and improvements	16
8. Conclusion.....	17
Flight simulator.....	17
1. Introduction	17
2. Background.....	17
3. Procedures	18
4. Discussion.....	19
5. Conclusion.....	19

1. Introduction

With modern aviation incorporating regular long-haul flights and the increasing fuel costs, an accurate navigation system is required in order to more precisely globally position the aircraft and reduce corrections required in the flight path to reduce the fuel consumption during flight. Several navigation systems can be used in order find the position of an aircraft during flight, most commonly the satellite based Global Positioning System (GPS) and local Inertial Navigation System (INS). GPS can give an accurate global position by triangulating the position of the aircraft relative to the satellites being used and is considered to be the most effective method of determining position, however, GPS is limited to only position and is unable to directly resolve the attitude and kinematics of the aircraft as well as having a very infrequent data acquisition rate. On the other hand, an INS uses an Inertial Measurement Unit (IMU) to reckon the position of the aircraft based on a set of initial parameters. The INS has a very high frequency data rate, however, the IMU integrates acceleration values to produce a velocity and position relative to the origin and is susceptible to accumulating errors. An IMU will be simulated to investigate the factors governing the response of a multi-degree of freedom model of an IMU and relate these to basic error prediction techniques.

2. Background

An Inertial Measurement Unit (IMU) within an INS method of dead reckoning can be assembled in many configurations with axis corresponding to several different measurements including an accelerometer (linear acceleration), rate gyroscope (Angular acceleration), and a magnetometer (direct orientation measurements). The IMU for simulation in this report will include a 3 axis rate gyroscope and a 3 axis linear accelerometer oriented in the orthogonal body x,y,z axis and yaw, pitch, roll axis. IMUs can be used in two main configurations, a platform mounted IMU which dynamically orients through the use of a gimbal to always maintain constant body frame to global frame alignment, and a strap down IMU which is aligned to the body frame and follows the attitude of the aircraft. For either implementation of IMU, the angular accelerations are integrated to give a change in attitude which can be integrated from a measured initial value to give the attitude as a function of time. The attitude dynamics can then be incorporated to find the NED components of the measured body accelerations for a strap down system which are then integrated to give the velocity and then again to give the position of the aircraft from initial measured conditions during setup procedures.

The simulation will be done of a strap down IMU which will require the incorporation of several general models including gravity, earth shape, earth rotation, relationship between navigational frames, rate of change of navigational frames, relation of local to global position and the constant change in attitude of the aircraft, as well as error dynamics. With the local orthogonal body axis, a mapping can be formed to the global North, East, Down, (NED) navigational frame and the shape of the earth can be seen as an oblate ellipsoid due to the centrifugal force from the earth rotation causing a larger radius over the equator as compared to the polar axis. A common model of the earth is that of "WGS 84" the World Geodetic System which is the standard earth model used for cartography and GPS navigation (Slater, 1998) and related the radius of the equatorial and polar planes by a value of flattening. After mapping of the local to global accelerations, the velocity and position of the IMU can be reckoned and translated into a global Longitude, Latitude, Altitude frame of reference.

The gravitational model of the earth can be represented as a function of height (h) from the surface of the earth with radius (r) and the gravity at the surface $g(0)$:

$$g(h) = \frac{g(0)}{\left(1 + \frac{h}{r}\right)^2} \quad (1)$$

With the gravity at the centre, $g(0)$, varying with latitude (λ) and constants $\alpha = 0.0053024$, $\beta = -0.0000058$ and $g_0 = 9.78$ (Allaby, 2008).

$$g(0) = g_0(1 + \alpha \sin^2 \lambda + \beta \sin^2 \lambda) \quad (2)$$

As previously mentioned, a model of the earth and its rotation can be assumed as an oblate ellipsoid (WGS 84).

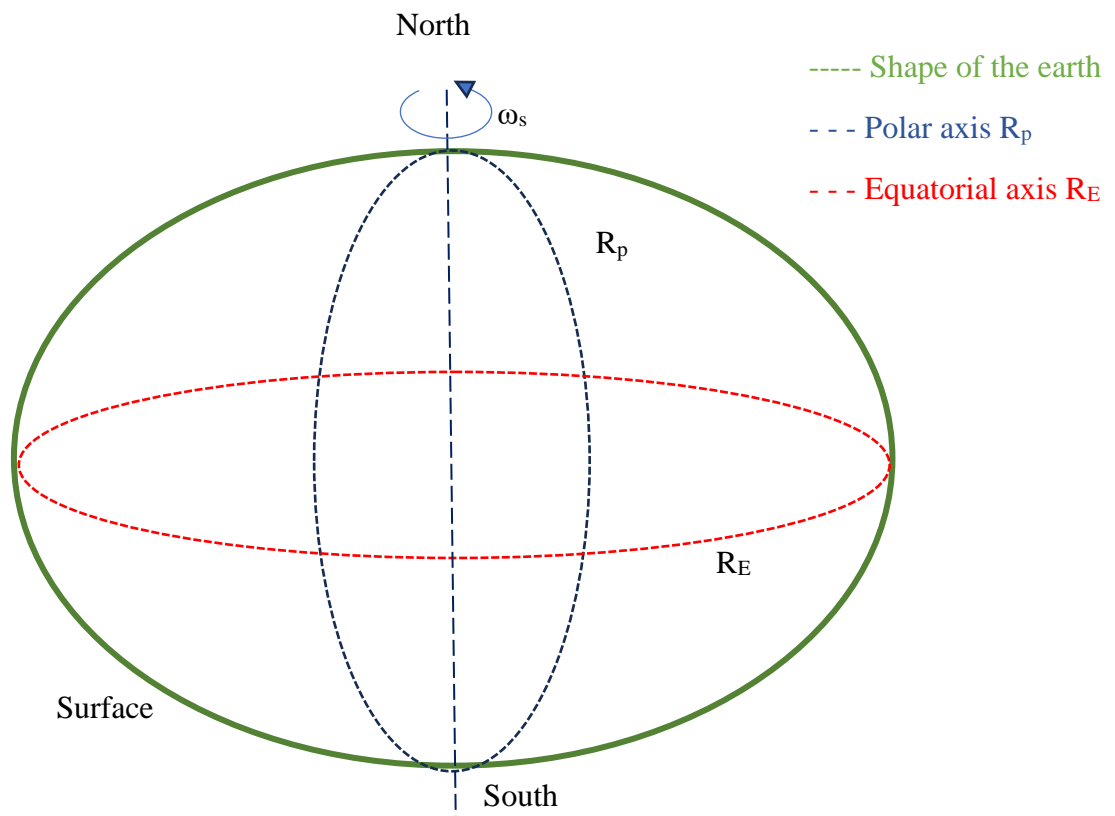


Figure 1: Geodetic earth diagram

R_p can be found to be 6356km and R_E to be 6378km with the Flattening, $f = 1/298.5$, relating the radius of the equator and polar axis as:

$$R_p = R_E(1 - f) \quad (3)$$

The eccentricity (e) can be related to the Flattening by:

$$e = \sqrt{f(2 - f)} \approx 0.08188 \quad (4)$$

Giving rise to the equations for the Meridian and Transverse radii of curvature, R_N and R_E respectively, in terms of the latitude and eccentricity:

$$R_N = \frac{R(1 - e^2)}{(1 - e^2 \sin^2 \lambda)^{\frac{3}{2}}} \quad (5)$$

$$R_E = \frac{R}{(1 - e^2 \sin^2 \lambda)^{\frac{1}{2}}} \quad (6)$$

The rotational side real rate (ω_s) can be found to be a constant for earth along the equatorial plane solely as:

$$\omega_s = 7.921158 \frac{rads}{day} \quad (7)$$

When assuming the earth as a perfect sphere, $R_p = R_E$ and:

$$R = R_p + h = R_E + h \quad (8)$$

As the linear and angular accelerations are a measured vector, they are susceptible to deviations and errors in readings as well as cumulative build up of error over time due to integration. The error in readings can be modelled with scaling errors (sc), misalignment errors (mis), true value (true), instrument bias (bias) and random error (rnd) with the matrices (M and S) and accelerometer (a) and gyroscope (gyr) sensors:

$$A_{meas} = (I + S_{a-sc})(I + M_{a-mis})A_{true} + A_{bias} + A_{rnd} \quad (9)$$

$$\omega_{meas} = (I + S_{gyr-sc})(I + M_{gyr-mis})\omega_{true} + \omega_{bias} + \omega_{rnd} \quad (10)$$

In order to represent the attitude of the aircraft a set of Euler angles is defined about the body axis as 1 the Roll (ϕ) about the x axis, 2 the Pitch (θ) about the y axis, and the Yaw (ψ) about the z axis. When translating the attitude of the axis from the body frame to the inertial frame, translations are carried out in the 3-2-1 (Paluszek, 2023). An inertial global frame is defined in the North East Down (NED) orthogonal orientation with the earth assumed to be plane and non-rotating in terms of the (NED) frame. The x axis is aligned to be positive towards the north axis and y to be positive towards the east axis with the z axis down towards the earth with the Latitude being the angle between the equatorial plane and the body, positive towards north, and the Longitude being the Distance from the Greenwich meridian line to the body, positive to the east. The relation between the local body frame and global NED frame can be represented with the transformation matrix T_{IB} transforming from body to inertial frame and angular velocity components p_b , q_b and r_b :

$$\begin{bmatrix} x_1 \\ y_1 \\ z_1 \end{bmatrix} = T_{IB} \begin{bmatrix} x_b \\ y_b \\ z_b \end{bmatrix}$$

Where:

$$T_{IB} = \begin{bmatrix} \cos(\psi) \cos(\theta) & \cos(\psi) \sin(\theta) \sin(\phi) - \sin(\psi) \cos(\phi) & \cos(\psi) \sin(\theta) \cos(\phi) + \sin(\psi) \sin(\phi) \\ \sin(\psi) \cos(\theta) & \sin(\psi) \sin(\theta) \sin(\phi) - \cos(\psi) \cos(\phi) & \sin(\psi) \sin(\theta) \cos(\phi) - \cos(\psi) \sin(\phi) \\ -\sin(\theta) & \cos(\theta) \sin(\phi) & \cos(\theta) \cos(\phi) \end{bmatrix} \quad (11)$$

With:

$$\dot{T}_{IB} = T_{IB} \begin{bmatrix} 0 & -r_b & q_b \\ r_b & 0 & -p_b \\ -q_b & p_b & 0 \end{bmatrix} \quad (12)$$

The angular velocity of the geographic NED frame can be represented as

$$\omega_g = \begin{bmatrix} \dot{\phi} \cos \lambda \\ -V_N \\ (R_p + h) \\ -\dot{\phi} \sin \lambda \end{bmatrix} \quad (13)$$

With the angular velocity of the body frame:

$$\omega_b = \begin{bmatrix} p_b \\ q_b \\ r_b \end{bmatrix} = \begin{bmatrix} 1 \\ 0 \\ 0 \end{bmatrix} \dot{\phi} + \begin{bmatrix} 0 \\ \cos \varphi \\ -\sin \varphi \end{bmatrix} \dot{\theta} + \begin{bmatrix} -\sin \theta \\ \sin \varphi \cos \theta \\ \cos \varphi \cos \theta \end{bmatrix} \dot{\psi} \quad (14)$$

And the attitude rates can be expressed as:

$$\begin{bmatrix} \dot{\phi} \\ \dot{\theta} \\ \dot{\psi} \end{bmatrix} = \begin{bmatrix} 1 & 0 & 0 \\ 0 & 1 & 0 \\ 0 & 0 & 1 \end{bmatrix} \begin{bmatrix} p_b \\ q_b \\ r_b \end{bmatrix} + \begin{bmatrix} 1 & \sin \varphi \tan \theta & \cos \varphi \tan \theta \\ 0 & \cos \varphi - 1 & -\sin \varphi \\ 0 & \frac{\sin \varphi}{\cos \theta} & \frac{\cos \varphi}{\cos \theta} \end{bmatrix} \begin{bmatrix} p_b \\ q_b \\ r_b \end{bmatrix} \quad (15)$$

During flight an aircraft is unaffected by the surface curvature of the earth, therefore a spherical earth model can be implemented at the height $r +$ altitude. The translation of the NED to the latitude, longitude, altitude frame can be done assuming a spherical earth model (8) giving the changes in latitude and longitude respectively as:

$$\dot{\lambda} = \frac{V_N}{R} \quad (16)$$

$$\dot{\phi}_L = \frac{V_E}{R \cos \lambda} \quad (17)$$

Incorporating the earth side real velocity which is parallel to the latitude and positive towards the positive latitudinal direction, making the change in latitude while in the air the difference between the two, and compensating for gravity, the spherical earth equations can be rearranged to give:

$$\begin{bmatrix} \dot{V}_N \\ \dot{V}_E \\ \dot{V}_V \end{bmatrix} = \begin{bmatrix} A_N \\ A_E \\ A_V \end{bmatrix} + \begin{bmatrix} 0 \\ 0 \\ g \end{bmatrix} - \frac{1}{R} \begin{bmatrix} 0.5\omega_s^2 R^2 \sin(2\lambda) + 2\omega_s R V_E \sin \lambda + V_E^2 \tan \lambda - V_N V_V \\ -2\omega_s R (V_V \cos \lambda + V_N \sin \lambda) - V_V V_E - V_E \tan \lambda V_N \\ \omega_s^2 R^2 \cos^2 \lambda + 2V_E R \omega_s \cos \lambda + (V_N^2 + V_E^2) \end{bmatrix} \quad (18)$$

And

$$\dot{\lambda} = \frac{V_N}{R}, \quad \dot{\phi}_L = \frac{V_E}{R \cos \lambda}, \quad \dot{h} = -V_V \quad (19)$$

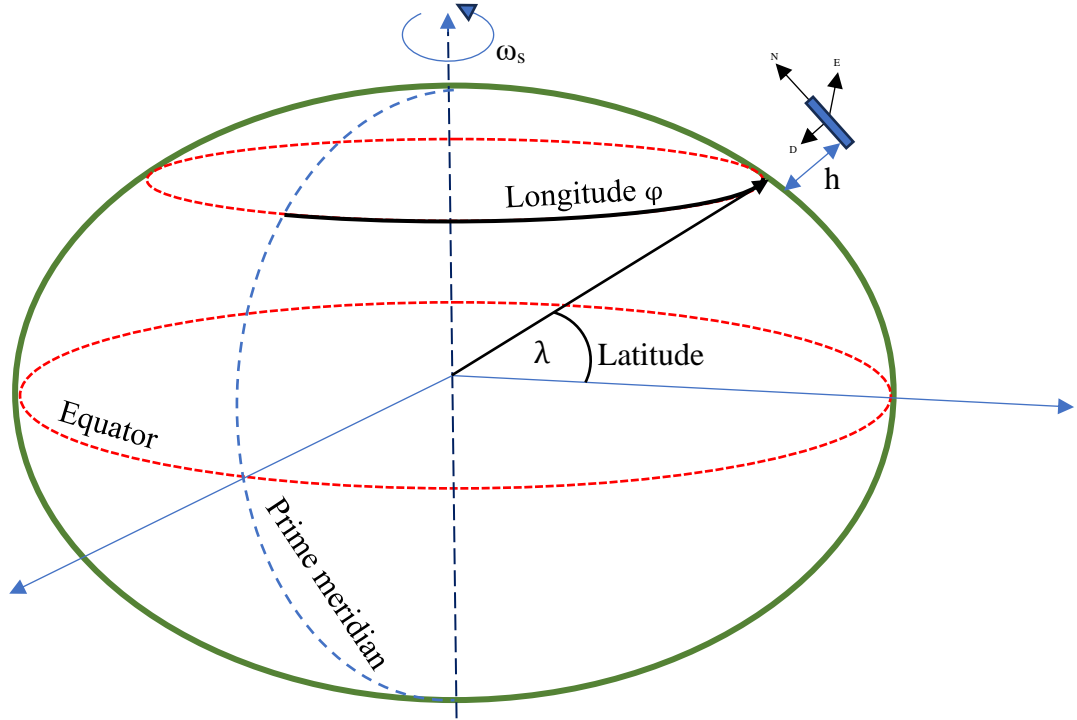


Figure 2: Diagram of Latitude and Longitude compared to NED

Additionally to the LLH frame, the NED frame can be represented in terms of the Earth Centred Inertial (ECI) frame where the origin is in the centre of the earth and the X axis points towards the Vernal Equinox, with various references e.g. the location of the equinox on Jan 1st 2000 (J2000), with the Y axis 90^o ahead of the X and the Z orthogonally oriented towards the north on the polar axis. As this reference frame is independent of the surface of the earth, another reference frame, the Earth Centred Earth Fixed frame (ECEF), can be used as an intermediary frame when converting from ECI to LLH as it maintains the Z axis from the ECI but aligns the X axis to the earth fixed prime meridian over Greenwich with the Y axis 90^o ahead of that. The relation between the ECI to ECEF is therefore the rotation ω_s about the Z axis with an approximate speed of 15^o/hr. This allows for an easy transition to the LLH frame as zero Longitude is on the prime meridian and zero latitude on the equator. It is also worth noting that while the meridian radius R_N is constant with travel, the longitudinal radius R_E is spatially dependent with Latitude with the relation, $R_E = R_N \cos(\lambda)$.

Giving the ECI to ECEF transformation matrix as:

$$T_{EI} = \begin{bmatrix} t \cos \omega_s & t \sin \omega_s & 0 \\ -t \sin \omega_s & t \cos \omega_s & 0 \\ 0 & 0 & 1 \end{bmatrix} \quad (20)$$

And therefore, the ECI to NED transformation matrix as:

$$T_{NI} = \begin{bmatrix} 0 & 0 & 1 \\ 0 & 1 & 0 \\ -1 & 0 & 0 \end{bmatrix} \begin{bmatrix} \cos \lambda & 0 & \sin \lambda \\ 0 & 1 & 0 \\ -\sin \lambda & 0 & \cos \lambda \end{bmatrix} \begin{bmatrix} \cos(\varphi_L + \omega_s t) & \sin(\varphi_L + \omega_s t) & 0 \\ -\sin(\varphi_L + \omega_s t) & \cos(\varphi_L + \omega_s t) & 0 \\ 0 & 0 & 1 \end{bmatrix} \quad (21)$$

And incorporating (13), (16), (17), the rate change of Body to NED frames, ω_{NB} , with the measured vector ω_B can be represented as:

$$\omega_{NB} = \omega_N - \omega_B = \begin{bmatrix} (\dot{\varphi}_L + \omega_s) \cos \lambda \\ -\dot{\lambda} \\ -(\dot{\varphi}_L + \omega_s) \sin \lambda \end{bmatrix} - \omega_B \quad (22)$$

Error dynamics of the IMU can begin to be modelled by representing a state vector q of the object in flight by:

$$q = [V_N \ V_E \ V_V \ \lambda \ \varphi_L \ h \ \psi \ \theta \ \varphi]^T$$

With the small perturbation errors of the state vector represented by:

$$\delta q = [\delta V_N \ \delta V_E \ \delta V_V \ \delta \lambda \ \delta \varphi_L \ \delta h \ \delta \psi \ \delta \theta \ \delta \varphi]^T$$

Expressing the NEV frame velocity error vector in terms of the body-NED transformation matrix and the body fixed accelerations and acceleration perturbations including the perturbations in earth's gravity, δg :

$$\begin{bmatrix} \delta \dot{V}_N \\ \delta \dot{V}_E \\ \delta \dot{V}_V \end{bmatrix} = \begin{bmatrix} 1 & 0 & 0 \\ 0 & 1 & 0 \\ 0 & 0 & -1 \end{bmatrix} (\delta T_{NB} A_B + T_{NB} \delta A_B) + \begin{bmatrix} 0 \\ 0 \\ \delta g \end{bmatrix} + \delta g_V \quad (23)$$

$$\delta \dot{\lambda} = \frac{\delta V_N}{R_p + h} - \frac{V_N}{(R_p + h)^2} \delta h \quad (24)$$

$$\delta \dot{\varphi}_L = \frac{\delta V_E}{(R_E + h) \cos \lambda} - \frac{V_E \delta h}{(R_E + h)^2 \cos \lambda} + \frac{V_E \sin(\lambda) \delta \lambda}{(R_E + h) \cos^2 \lambda}, \quad (25)$$

$$\frac{d\delta h}{dt} = -\delta V_V \quad (26)$$

And the perturbation in the Transformation matrix T_{NB} can be represented through:

$$\delta T_{NB} = \tilde{T}_{IN}^T T_\theta^T \delta T_\theta^T + \tilde{T}_{IN}^T \delta T_\theta^T T_\theta^T + \delta \tilde{T}_{IN}^T T_\theta^T T_\theta^T \quad (27)$$

From the measured acceleration values in (9) & (10) the perturbations in the true body fixed frame accelerations can be derived as:

$$\begin{aligned} \delta A_B = & (-M_{a-mis}^{-1} \delta M_{a-mis} (I + M_{a-mis})^{-1} - (I + M_{a-mis})^{-1} S_{a-sc}^{-1} \delta S_{a-sc}) (I + S_{a-sc})^{-1} \\ & * (A_{mea} - A_{bias} - A_{rnd}) + (I + M_{a-mis})^{-1} (I + S_{a-sc})^{-1} (\delta A_{meas} - \delta A_{bias} - \delta A_{rnd}) \end{aligned}$$

Where measured perturbations of acceleration can be measured during calibration and misalignment and scaling errors can be approximated by the position of the IMU within the aircraft body, in relation to its centre of gravity (centre of rotation), and the nominal error values of the integrators used. Bias errors can be minimized during initialization however due to their nature, particularly in terms of the gyro bias, the error propagates due to the integrators and is the leading contributor in the drift values of the IMU. The IMU drift is the gradual deviation between measured and true values and the position errors can be predicted with the polynomial relation to be proportional to time³. In a perfectly aligned IMU and no scaling error:

$$\delta A_B = \delta A_{meas} - \delta A_{bias} - \delta A_{rnd} \quad (28)$$

3. Block diagrams and subsystems

NED to navigation frame transformation subsystem

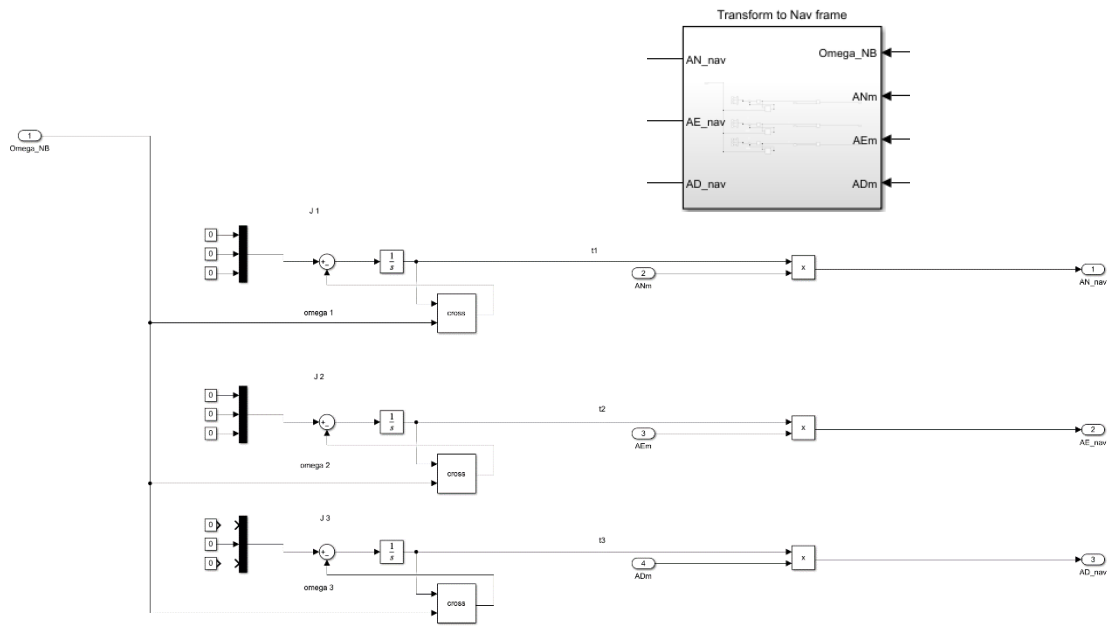


Figure 3: NED to navigational frame

Angular velocity of the NED frame

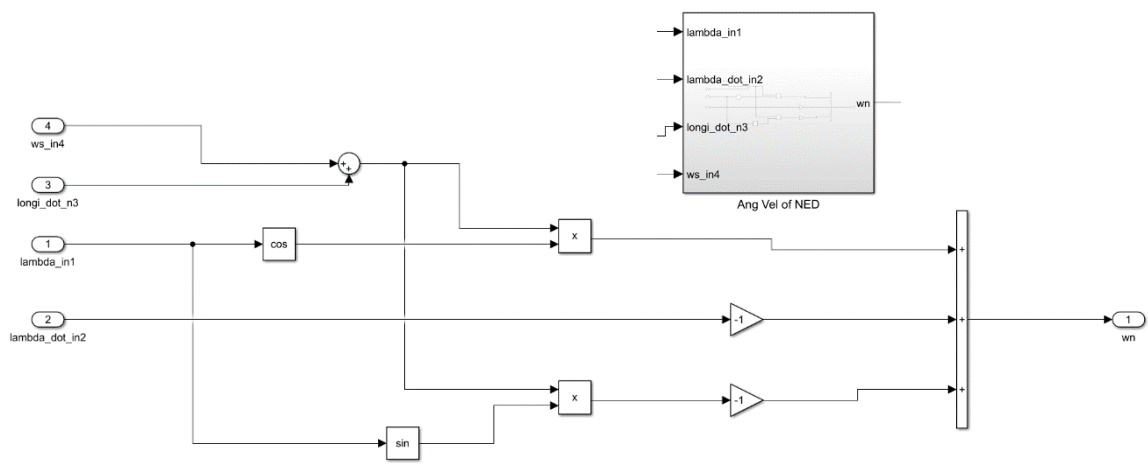


Figure 4: Angular velocity of the NED frame

NEV velocity from accelerations

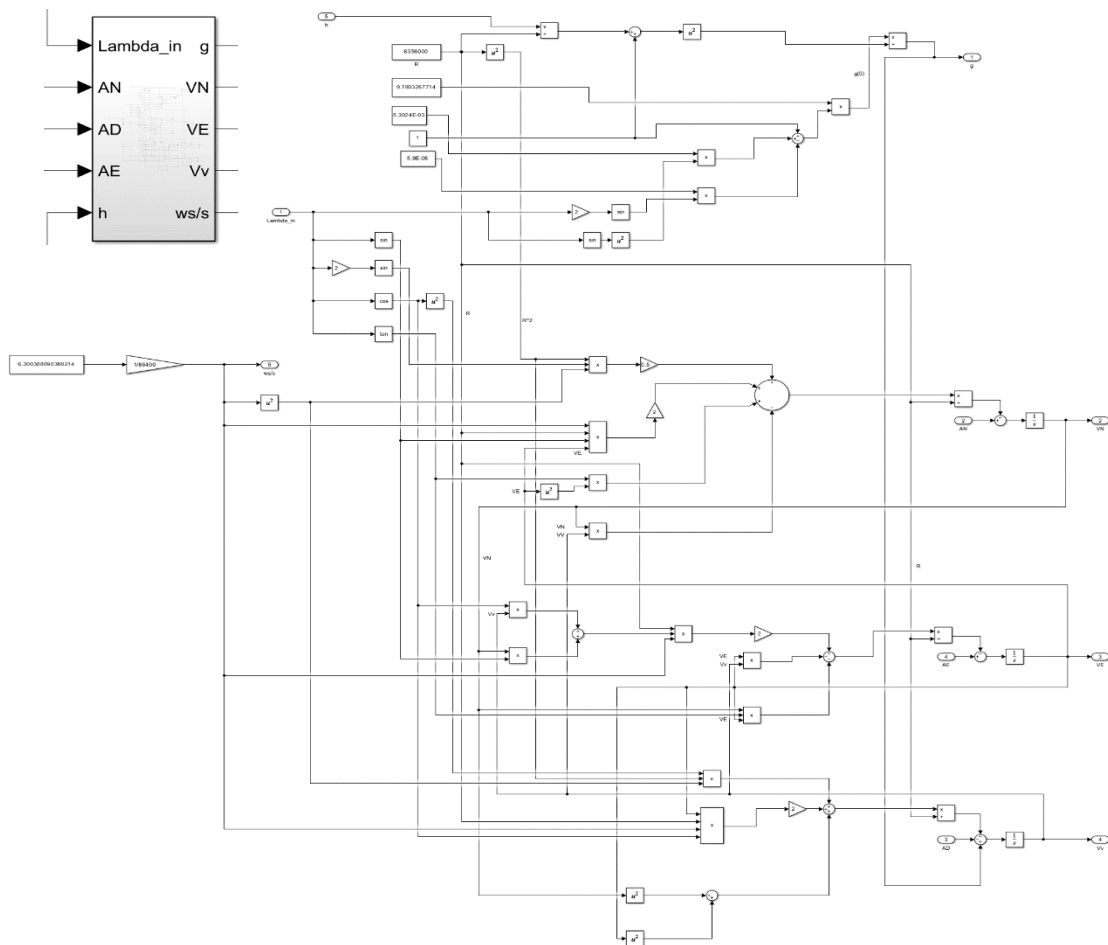


Figure 5: Velocity from accelerations

Velocity to position calculations

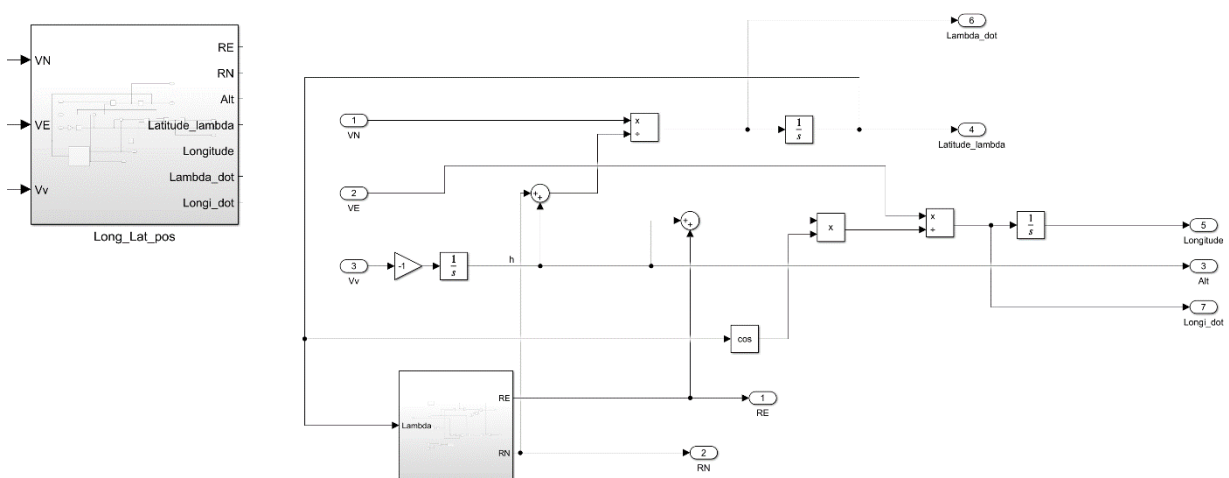


Figure 6: Velocity to position

Radius component calculations, R_E and R_N

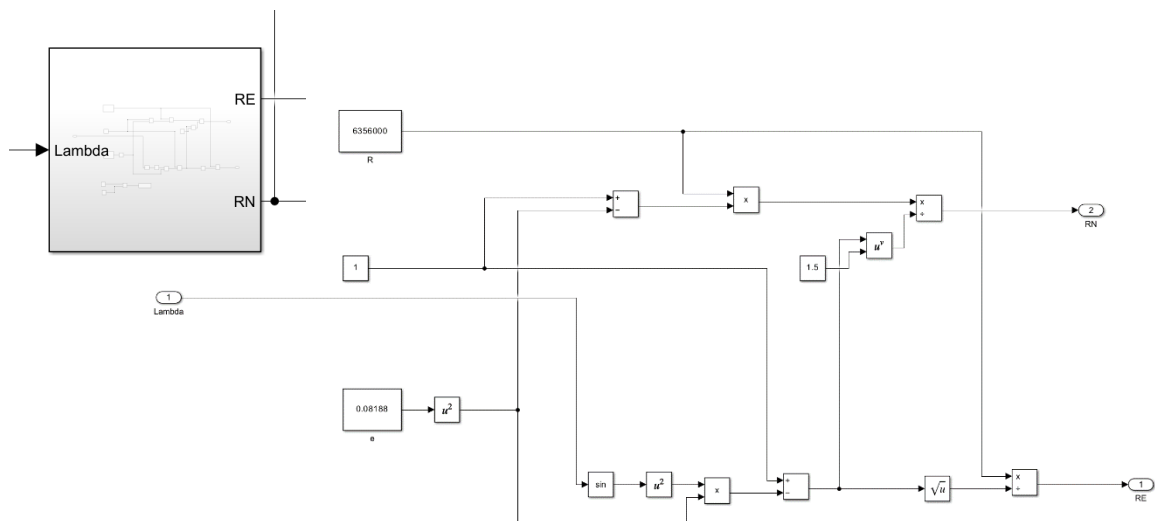


Figure 7: R_E and R_N from λ

Measured simulation block

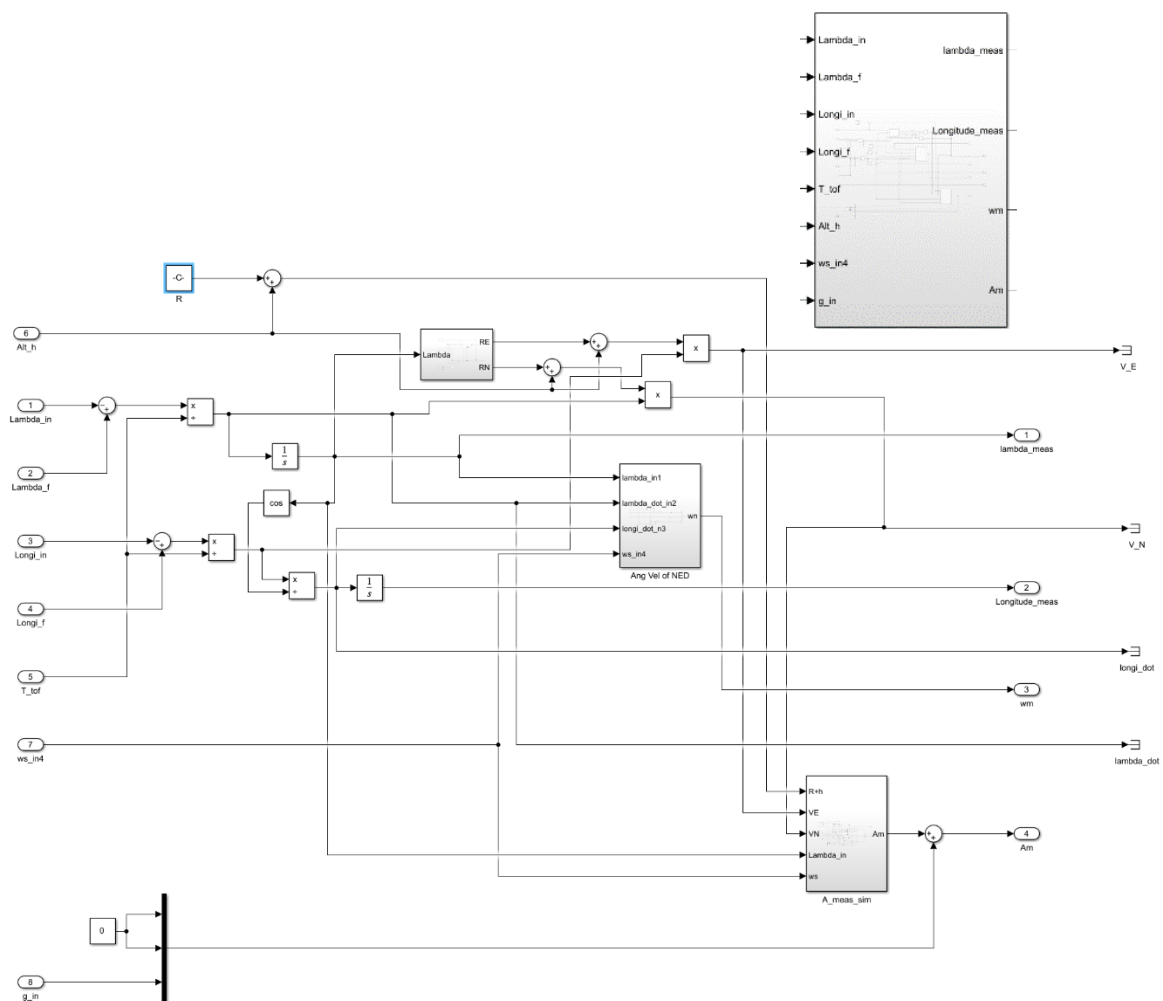


Figure 8: Simulation block

Simulation of measured accelerations

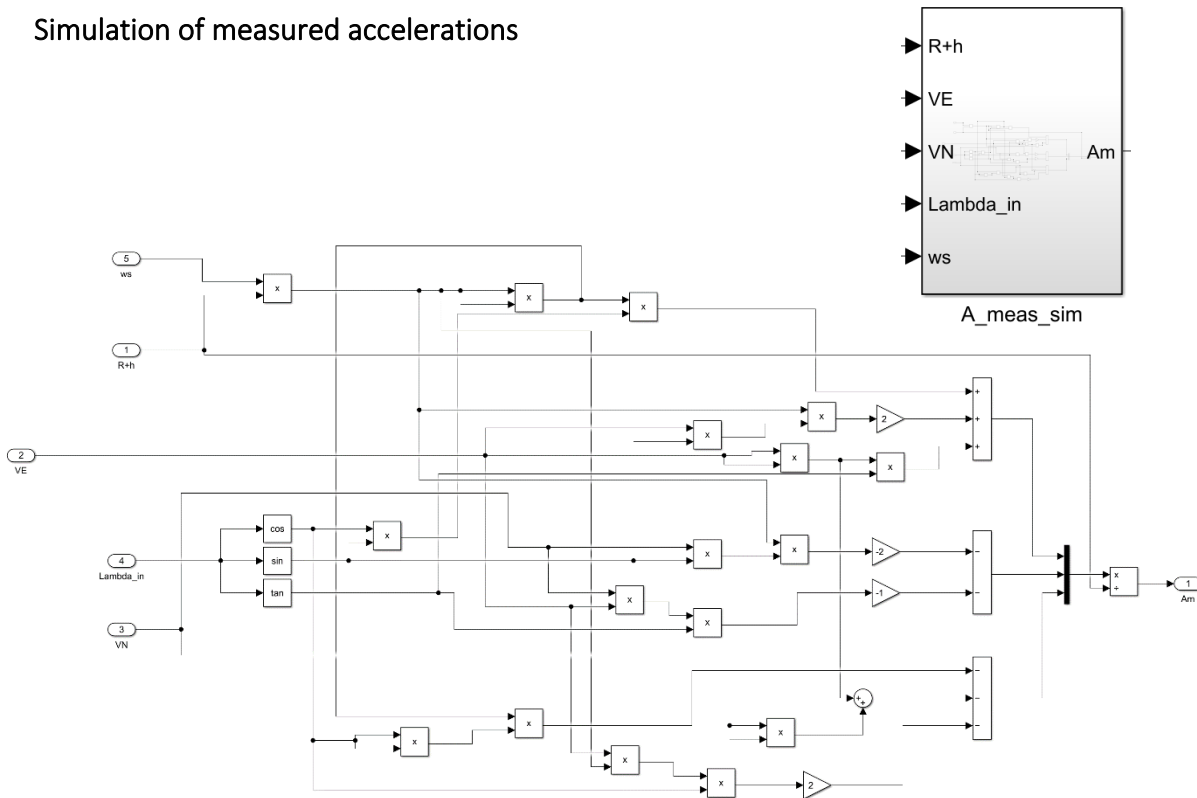


Figure 9: Simulation of accelerations

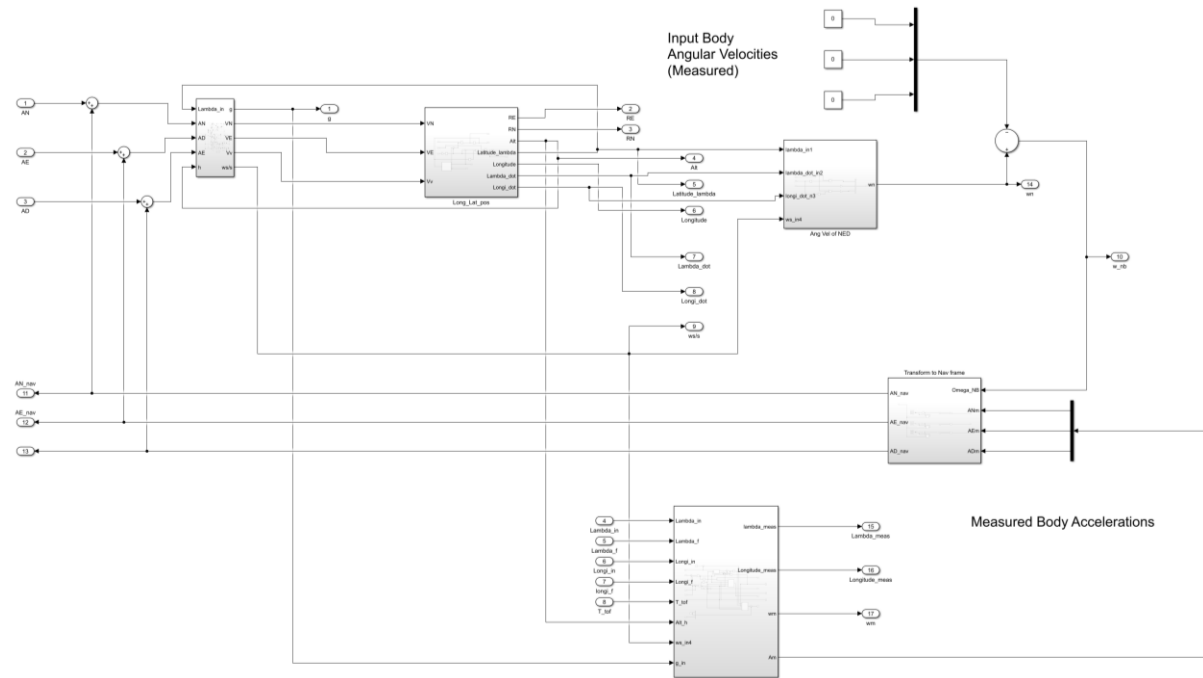


Figure 10: Block diagram overview

4. Testing

After successful modelling of the IMU within MatLab/SIMULINK testing of the system is conducted for two scenarios of steady level flight of an aircraft to analyse the factors governing the response of a multi-degree of freedom model of an IMU and relate these to basic error prediction techniques.

Flight scenarios and Initial conditions:

- 1) London to Amsterdam
- 2) London to Glasgow

Table 1: Location Latitude and Longitudes

	Latitude (radians)	Longitude (radians)
London	0.899016741506	-0.0020610942203
Amsterdam	0.914167787662	0.0854699952
Glasgow	0.974956907378	-0.074201503778

Table 2: Mission profiles for simulation

	$\Delta\lambda$ (radians)	$\Delta\Phi$ (radians)	Alt (m)	Time of Flight (s)	V_N (m/s)	V_E (m/s)	V_V (m/s)	$A_V \max$ (m/s ²)
London Amsterdam	- 0.01515104616	0.08753108942	10000	3600	26.78	94.69	0	-9.782
London Glasgow	- 0.07594016587	-0.07214040956	10000	3600	134.3	-71.76	0	-9.785

Assuming perfect alignment of the IMU with the aircraft centre of gravity and the positive x direction of the aircraft, and a perfectly efficient computational integration method with no scaling error, a set of arbitrary initial error values can be defined and used with (23 – 28):

Table 3: Error values

Type	Value
Attitude	± 0.050383292182 (max 0.0872665), radians
Velocity	± 1 m/s
Position	± 1 m
Rate Gyro bias (drift)	$\pm 0.0523599 - 0.00349066$ radians
Rate Gyro rnd	$\pm 1 \sigma$
Accelerometer bias	$\pm 0.01g$
Scaling and Alignment	0

5. Results

For an ideally perfect IMU the following graphs show the flight path for flight 1:

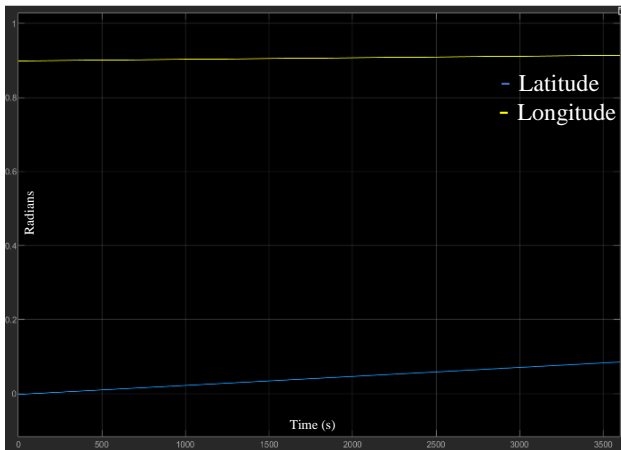


Figure 11: Latitude and Longitude with time for flight 1

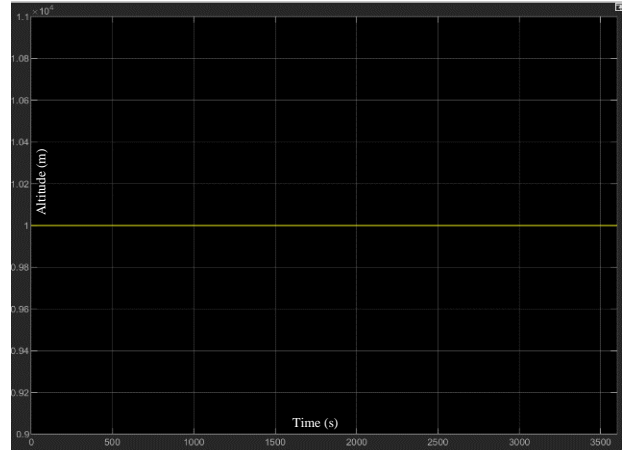


Figure 122: Altitude with time for flight 1

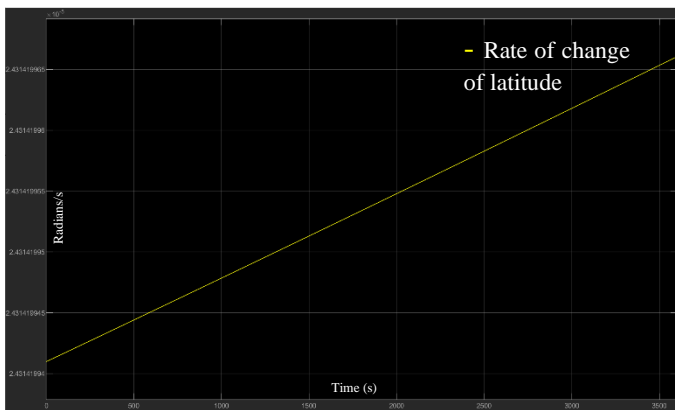


Figure 133: Rate of change of Longitude and Latitude for flight 1

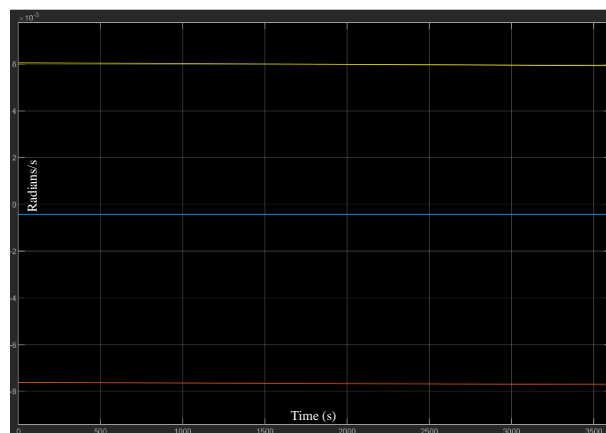


Figure 14: Angular velocity of NED and Body frames for flight 1

When error values are taken into account, the flight path measured are shown below:

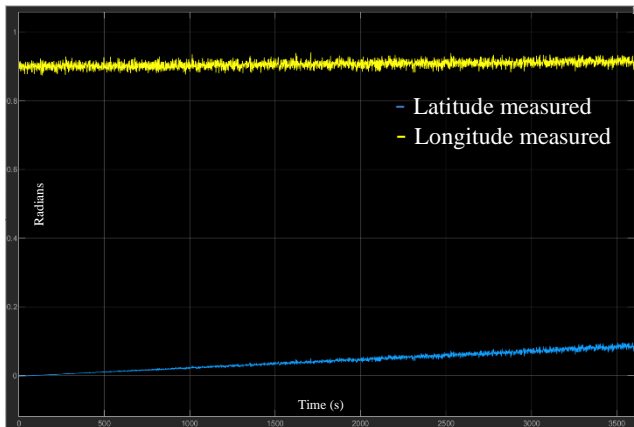


Figure 15: Measured Latitude and Longitude with time for flight 1

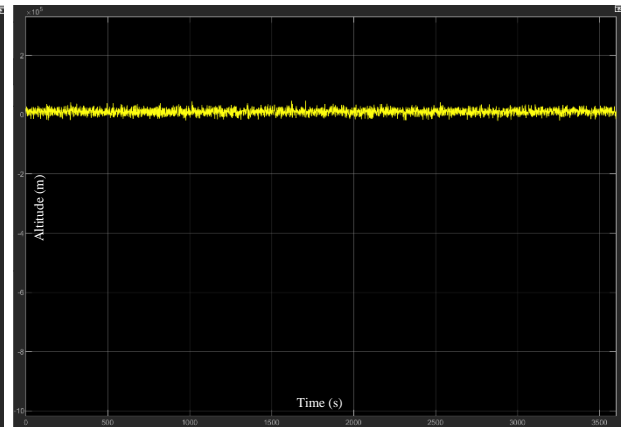


Figure 16: Measured altitude for flight 1

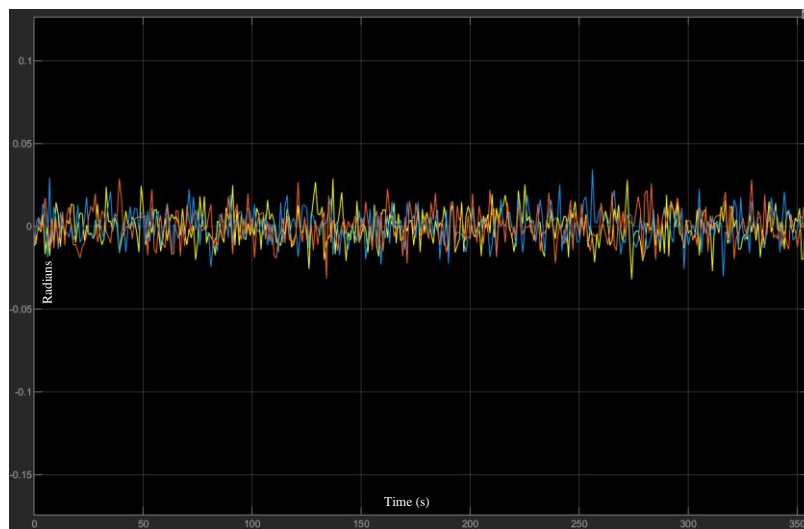


Figure 17: Measured velocity of NED and Body frames

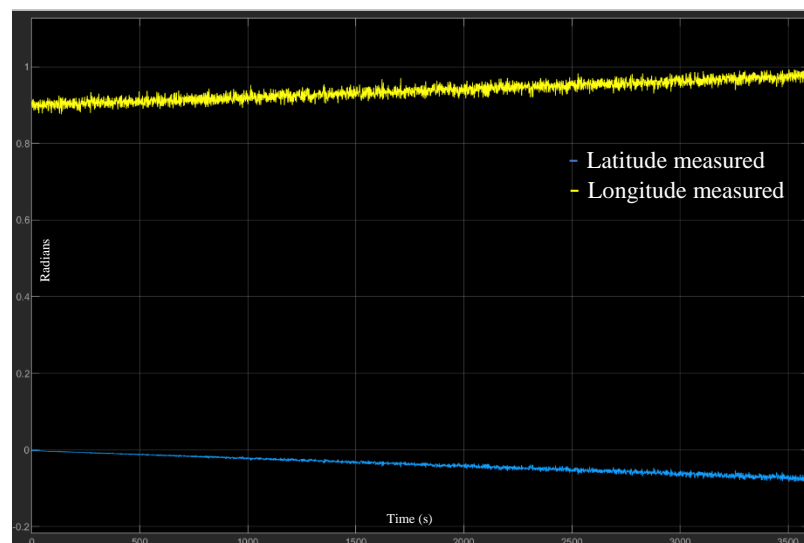


Figure 18: Measured Latitude and Longitude for flight 2

6. Discussion

This paper set out to create a simulation of the IMU unit within an Inertial Navigation System for an air vehicle, taking into account freedom of movement in 3 axis. The flight conditions of an aircraft at steady level flight at 10km altitude over a time of flight of 1hr was simulated over 2 flight profiles to determine the validity of the simulation. At first the exact flight path was simulated for each flight in order to act as the inputs to the simulator for which the measured Longitude, Latitude, Height and Angular velocities could be calculated. The error and measured value equations along with the assumed error values can be found in section 4 with the results of the flight data also given. From the results of the flight path it can be seen that the Latitude changes linearly with time with a constant velocity, however due to the curvature of the earth and the oblate geodetic shape, the Longitude change is not linear with time since the curvature is dependent on the Latitude. As the Latitude increases, the Easterly radius of the earth decreases, shown in figure 2, and the change in geodetic Longitude with a constant Easterly velocity results in the increase in rate of change of Longitude over time, which is in agreement with the WGS 84 model of the earth. Additionally, it can be seen that when correcting for gravity and assuming the accelerator values to be negligible and the direct over the ground flight path being straight, the angle of the NED and Body frames is in constant rotation. The measured value is near negligible with a magnitude of -6, this can be explained as while the Longitude and Latitude are changing, the geographic orientation of the aircraft due to the earth model also changes, as the journeys are relatively short this results in a constant but minimal overall change.

When simulating values, it can be seen that there are fluctuations in the measured values which increase over time, and the final values show the aircraft arriving at a different Latitude and Longitude than what was expected. This introduces an aspect of uncertainty in the aircrafts location when based solely on the INS which increases over time. This can be explained by the nature of the Inertial Measurement Unit which uses a method of dead reckoning to approximate a position based off of initial conditions (Flenniken, 2005). The accelerometer and rate gyro incorporated in the IMU are 3 axis each and measure the perceived linear and angular accelerations, which are susceptible to fluctuations due to several factors including noise within the circuitry, magnetic fluctuations in the environment, fluctuations in gravitational forces and vibrations. For the purpose of the simulator these were modelled as random noise, A_{rnd} , ω_{rnd} , as they are unpredictable but can generally be assumed to be within an arbitrary range as previously experimentally established. On the simulation results this can be seen as the rapid oscillations in values of Longitude, Latitude and Height. Additionally to this as the IMU is a physical instrument, it is vulnerable to errors in readings where a small change is measured in one direction when it is not in fact being experienced, this is often due to imperfections in manufacturing and is referred to as a bias error, A_{bias} , ω_{bias} , where it is often not a fluctuating value. On the measured simulation results this can be seen as a slight deviation on the average measured Longitude, Latitude and Height at a given time leading to a different final value. This phenomenon of the bias can be referred to as the Drift of the system as the value “drifts” away from the true value over time.

The resultant graphs of the simulation also show the fluctuations and errors increasing over time, this propagation of error is due to the underlying mechanism of the double integration to convert acceleration values to velocities to then position changes. The errors are fed into the integrators, amplified and accumulated over time, meaning that even small errors can present

significant uncertainties over a prolonged period which is the primary reason in which INS systems are often not used as stand-alone methods since they can only accurately be implemented over relatively short periods.

While for the test case the alignment and scaling errors were assumed to be negligible, it is worth noting that for aircraft this is generally not the case. For scaling errors, S_{sc} , they stem from similar sources as the bias and random errors, as physical instruments are not capable of producing perfectly calibrated and exact values even given the same calculations. The scaling errors can be defined as the errors due to imperfections in the methods of integration. The alignment errors for an aircraft generally present a significant issue as aircraft do not have a constant mass during flight, therefore their centre of gravity and centre of rotation are subject to change over a given flight. This means that even if an IMU axis is aligned perfectly with the aircrafts orthogonal axis and positioned at the centre of gravity, which is rarely the case, the alignment error may start at zero but as the aircraft burns fuel and its centre of gravity changes, the alignment of the axis will change, and the alignment error will increase.

As previously discussed, the error and uncertainty in INS based position over time increases over the local space, however additionally to this in a global reference of a long-haul flight, the significant change in global position further adds to the error due to the radius of the earth and constant change in attitude. An IMU system requires the compensation of the gravitational acceleration which is constantly changing direction in an oscillatory pattern. This was a phenomenon first discovered by Maximilian Schuler, where the oscillatory period can be determined as the period of a pendulum of length equal to the radius of the earth (Wrigley, 1950). This Schuler Pendulum moment defines the oscillation period of 84 minutes which also dictates several other phenomena such as a low orbit satellite period and several other gravity dependent cases. For the case of Schuler tuning an INS, errors can be seen to oscillate to the Schuler 84 minute period and as such updates to error values can be taken at this period in order to update the accuracy of assumed position.

7. Limitations and improvements

While an IMU has its benefits in terms of being an isolated independent system with a high refresh rate and adequate accuracy in the modern age, there are several limitations for the sole use of inertial navigation. Many of the drawbacks of an INS stem from the uncertainty of a position which can be accounted for by the incorporation of a joint GNSS/INS system which uses GPS for absolute position, with a IMU for attitude and also navigation for any areas with loss of GNSS signal. The errors on an INS can also be reduced by the implementation of a more modern laser IRS in place of the IMU (Petricoli, 2014) which uses the more reliable Sagnac effect (Post, 1966) for its rate gyros, reducing drift error and uncertainty.

The simulation carried out was largely a success for the 6 axis combined IMU in question and for an average INS with an error of 0.1NM/hr it can be seen that for an hour flight as in this simulation, the expected uncertainty is approximately $\pm 0.1\text{NM}$ which is very acceptable but in a case of a long haul flight of approximately 14 hrs, the resultant uncertainty is 1.4 NM which will severely impact the final approach and landing procedures. In terms of limitations of the simulator created, the error prediction principles could use further improvements in future to use principles such as Kalman filtering in order to better predict the final position, incorporating estimated states to be compared to measurements to allow for future refinement in compensation of estimations (Maybeck, 1990). Additionally as the simulation used the Euler

angle transformation of attitude and frames, it is mathematically limited as there are trigonometric functions in the denominators of many of the significant transformation equations meaning that several zero division errors will occur potentially crashing the software. For the scope of this simulation this was not an issue however for a satellite or flight which could be passing close to the poles or performing large attitude manoeuvres, such as a fighter jet, a quaternion implementation will be required. Quaternions use complex numbers to substitute all calculations to use only multiplication (Goldman, 2011) removing the possibility of a zero-division error, the use of quaternions also solves the problem of gimble lock, (Hemingway, 2018) where two axis align and a degree of freedom is lost, as it removes the orthogonal Euler vectors.

8. Conclusion

A simulation of a general IMU was implemented using the block diagram MatLab/SIMULINK of a three axis of freedom accelerometer and rate gyro bundle. The simulation took a set of predefined error values to generate the Latitude, Longitude and Altitude for two flight scenarios of steady level flight over a 1hr duration at 10km altitude. The simulation accurately represented the flight path for each mission profile and the measured values showed good agreement with the expected errors, showing the random fluctuations and drift of values with time.

Flight simulator

1. Introduction

Flight simulators have been used since the early days of aviation in order to train pilots for advanced and emergency manoeuvres as well as providing flight time when aeroplanes are not available or there are insufficient funds for the operating costs of training flights. Modern simulators provide sensory feedback through a dynamic platform and visual feedback through a in cockpit display which together create a life like illusion of the forces experienced during flight, however there are several limitations to their capabilities. This paper investigates and discusses the benefits and drawbacks of modern systems as well as the errors and observations taken from the use of a multi degree of freedom simulator.

2. Background

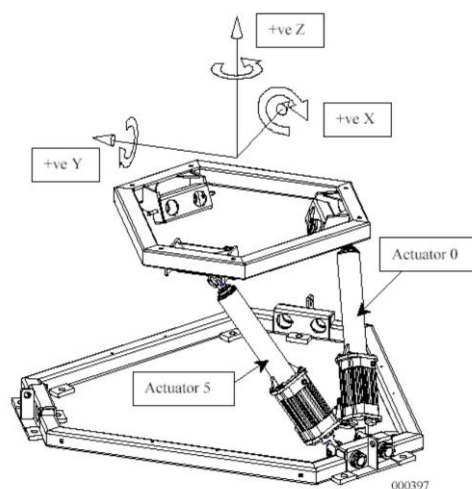


Figure 19: Stewart Platform diagram (Vepa, 2008)

The simulator in use is the CueSim Explorer RD simulator of an F-16 fighter jet mounted on a Stewart platform with six degrees of freedom (Figure 19). The platform is able to simulate the g-load, angular accelerations and angular speed sensations which would similarly be experienced during a flight. The platform consists of six linearly variable actuators supporting a cockpit (Nanua, 2003) with a visual display, audio feedback, centre control stick, control pedals and throttle, among other control devices. The simulator allows users to carry out manoeuvres while experiencing an accurate representation of the forces which would be experienced while reducing all the risks of crashing as the simulator can quickly be reset.

There are several reasons a dynamic simulator is desirable over a stationary alternative, these are due largely to the additional vestibular illusions which are experienced through the Stewart platform. The dynamic platform allows for practical training where spatial disorientation can be studied and trained on in a safe manner. The spatial disorientation types being;

Type 1 (unrecognized)

The pilot does not perceive spatial disorientation and may not be aware of attitude changes, which if combined with a false sense of security meaning that they are not checking their instruments, could lead to a fatal incident.

Type 2(recognized)

The pilot may realise there is a problem but trust their perception over the flight instrumentation and failing to correct for their errors.

Type 3(Incapacitating)

The pilot is under such spatial disorientation that they are no longer able to safely operate the aircraft.

Of these, type 1 is accepted to be the most dangerous as a fatal error could occur before any of the flight staff has had a chance to account for it.

Flight simulators also allow the pilot to experience a common skill gap among new pilots which is that of Pilot Induced Oscillation. This occurs when a pilot will fight the natural stability of the aircraft creating an oscillation in their attitude during flight, which mainly poses an issue for landings. The most common form would be due to a pilot misjudgement, where they miscalculate their height on approach and repeatedly over correct.

3. Procedures

The supporting systems of the simulator including the software on the Host PC, internal HUD displays and the motion control card must first be initiated. After which the pilot is able to enter the cockpit where they secure themselves with a harness to the chair in the simulator, communication with the external controller is established and the Stewart platform may then be engaged. The platform will rise from a standby position to an initial position of steady level flight, at which point the throttle can be increased and the pedals can be used to maintain a straight path down the runway. The control stick is used to control the simulated aircraft attitude changes corresponding to changes in flight control surfaces. The pilot will then carry out the specified set of manoeuvres designed to highlight situations where the pilot's intuition and sensory queues may disagree with the aircraft instrumentation. Observations are recorded to then form the analysis of this report.

4. Discussion

The flight simulation exercise was conducted for a test flight of several manoeuvres including landings and take-offs. The Stewart platform performed the expected attitudinal adjustment with minimal latency to provide accurate sensory feedback to the pilot. The g-loading on the pitching manoeuvres was notable and the attitude of roll in a banked turn accurately captured the expected sensations. Limitations were noticed on the banked turn where the g-loading is unable to be sustained during large radius turns as the Stewart platform is incapable of producing full rotations. This also meant that the negative g-loading on roll manoeuvres when upside down is un-capturable as the simulator can not produce a large angle of roll. During roll manoeuvres, the roll sensation was felt throughout the roll even though the simulator could not actually physically perform this, which can be explained as the vestibular system detects acceleration and not velocity meaning that a sharp initial roll with a sustained ocular illusion provides the roll sensation throughout the entire roll. At times when rolling was occurring and returning back to level flight, the illusion of steady level flight and the Leans could be observed and a Type 1 disorientation can be seen to occur. Types 2 and 3 were not present throughout the simulation and are largely dependent on the individual pilot.

On landings the dangers of inexperience are quickly observed as the high sensitivity of the F-16 meant that over-correcting the attitude on landing was a common mistake taking place and while in this instance did not lead to what would have been a fatal incidence, it led to sub-optimal landings. In a best-case scenario, the pilot would realise the accumulation of PIO and allow the aircraft to return to a steady state, at which point a go-around can be initiated for another attempt at a safer landing. When this was not the case, it led to the aircraft having heavy landings and harsh deceleration on landing, reducing the life span of the landing gear, potentially increasing the number of general services the aircraft would go through and increasing the in-service costs of the aircraft. In order to fully assess the capability of the simulator in future, a trained pilot can be acquired to perform latitudinal and longitudinal modes such as spirals and Dutch rolls, while also contributing their previous experience of aircraft handling and sensory feedback.

5. Conclusion

A simulation exercise was carried out of an F-16 fighter jet in the CueSim Explorer, Stewart platform mounted, simulator and several vestibular illusions were experienced with the dangers of PIO being observed. The ocular and vestibular combined illusions provided a good overall sensation of the load factors and dynamics experienced through flight.

References

- Allaby, M. (2008). A dictionary of earth sciences. Oxford ; New York: Oxford University Press.
- Petritoli, E. Giagnacovo ,T. and Leccese,F. (2014) "Lightweight GNSS/IRS integrated navigation system for UAV vehicles," IEEE Metrology for Aerospace (MetroAeroSpace), Benevento, Italy, 2014, pp. 56-61, doi: 10.1109/MetroAeroSpace.2014.6865894.
- Flenniken, Warren S., IV, Wall, John H., Bevely, David M.,(2005) "Characterization of Various IMU Error Sources and the Effect on Navigation Performance," Proceedings of the 18th International Technical Meeting of the Satellite Division of The Institute of Navigation (ION GNSS 2005), Long Beach, CA, September 2005, pp. 967-978.
- Goldman, R. (2011). Understanding quaternions. Graphical Models, 73(2), pp.21–49. doi:<https://doi.org/10.1016/j.gmod.2010.10.004>.
- Hemingway, E.G., O'Reilly, O.M. (2018). Perspectives on Euler angle singularities, gimbal lock, and the orthogonality of applied forces and applied moments. Multibody Syst Dyn 44, 31–56 <https://doi.org/10.1007/s11044-018-9620-0>
- Maybeck, P.S. (1990). The Kalman Filter: An Introduction to Concepts. In: Cox, I.J., Wilfong, pp.431-437, G.T. (eds) Autonomous Robot Vehicles. Springer, New York, NY. https://doi.org/10.1007/978-1-4613-8997-2_15
- Nanua,P. Waldron, K.J. (2003). Direct kinematic solution of a Stewart platform. doi:<https://doi.org/10.1109/robot.1989.100025>.
- Paluszek, M. (2023). ADCS - Spacecraft Attitude Determination and Control. Elsevier. 581-602
- Post, E.J. and Force, A. (1966). The Sagnac effect. L.G. Hanscom Field, Massachusetts: Air Force Cambridge Research Laboratories, Office Of Aerospace Research, United States Air Force.
- Slater, J.A., Malys, S. (1998). WGS 84 — Past, Present and Future. In: Brunner, F.K. (eds) Advances in Positioning and Reference Frames. International Association of Geodesy Symposia, vol 118. Springer, Berlin, Heidelberg. https://doi.org/10.1007/978-3-662-03714-0_1
- Vepa, R, “Aircraft flight simulation exercise,” DEN7001/ DENM001 Advanced Flight Control and Simulation of Aerospace Vehicles, pp. 1–24, 2008.
- Vepa, R, “Aircraft flight simulation exercise 2,” DEN7001/ DENM001 Advanced Flight Control and Simulation of Aerospace Vehicles, pp. 1–24, 2021.
- Wrigley, Walter (1950). SCHULER TUNING CHARACTERISTICS IN NAVIGATIONAL INSTRUMENTS. Navigation, 2(8), 282–290. doi:10.1002/j.2161-4296.1950.tb00579.x